The five restraints discussed above are easily introduced into refinement procedures and suitable additions to the *PROLSQ* algorithm to prevent unacceptable hydrogen bonding and apply to neutron as well as X-ray data.

The original CO-myoglobin data was collected in collaboration with A. C. Nunes and J. C. Norvell. The original coordinates of myoglobin were provided by J. C. Kendrew and H. C. Watson. We are grateful to Drs A. J. Wonacott and R. Knott for helpful discussions and critically reading the manuscript. The work was supported by the Office of Health and Environmental Research and the calculations were performed under the Supercomputing Program of the United States Department of Energy.

References

CHENG, X. & SCHOENBORN, B. P. (1990). *Acta Cryst.* B**46**, 195-208.
HENDRICKSON, W. A. (1985). *Meth. Enzymol.* **115**, 252-270.
HENDRICKSON, W. A. & KONNERT, J. H. (1981). In *Biomolecular Structure, Function, Conformation and Evolution*, Vol. 1, edited by R. SRINIVASAN, pp. 43-57. Oxford: Pergamon.
KONNERT, J. H. (1976). *Acta Cryst.* A**32**, 614-617.
SAVAGE, H. F. J. & FINNEY, J. L. (1986). *Nature (London)*, **322**, 717-720.
SCHOENBORN, B. P. (1988). *J. Mol. Biol.* **201**, 741-749.

Acta Cryst. (1991). A**47**, 317-327

Theoretical and Experimental Studies of Electron Resonance Effects in Reflection High-Energy Electron Diffraction

BY P. LU,* J. LIU AND J. M. COWLEY

Department of Physics, Arizona State University, Tempe, AZ 85287, *USA*

(*Received* 3 *April* 1990; *accepted* 11 *September* 1990)

Abstract

The electron resonance effect for 100 keV electrons incident on the surface of GaAs (110) in RHEED is studied by theoretical simulations using multislice theory and experimental observations. The exact resonance conditions, effective resonance region, effective penetration depth of electrons at or near the resonance condition and scattering processes involved for the resonance effect are investigated. It is found that the intensity of the 440 specularly reflected beam is mainly due to direct reflection from the surface atomic layer and beam enhancement due to surface channeling effects under the resonance conditions seems to be insignificant. For the 880 specularly reflected beam most of the electron intensity penetrates the surface and is diffracted by the crystal. The resonance condition for the 880 specular beam is satisfied when the transmitted beam excites a strong surface wave which propagates in the direction parallel or nearly parallel to the surface and is localized in the surface region by the surface potential barrier; double diffraction from the surface beam to the specular beam then enhances the total intensity in the specular beam. The exact resonance condition for the 880 beam is found to be at the glancing angle of 35·7 mrad and the azimuth angle of 29·7 mrad. A strong wave field is localized in the surface region at the resonance condition with an effective electron penetration depth of ~5 Å, which increases to ~35 Å on going to the nonresonance conditions. The effective resonance region for the 880 spot is ~2 mrad about the azimuth angle and ~1 mrad about the glancing angle.

1. Introduction

The technique of reflection electron microscopy (REM), in which a high-energy electron beam (20-200 keV) is incident on a surface at a glancing angle of 1-2° and forms a reflection high-energy electron diffraction (RHEED) pattern, is now becoming one of the most important microscope methods for investigating surface structures (Yagi, 1987). The REM image which is formed by selecting one of the reflected beams provides structural information about the surface (Yagi, 1987) and electron energy-loss spectroscopy (EELS) with the reflected beams can provide complementary chemical information (Krivanek, Tanishiro, Takayanagi & Yagi, 1983; Howie, 1983; Wang & Cowley, 1988). It has been found that the

* Present address: Department of Mechanics & Materials Science, Rutgers, Piscataway, NJ 08855-0909, USA.

0108-7673/91/040317-11$03.00

contrast and quality of REM images and observations of the EELS spectrum are strongly influenced by the electron diffraction condition (Uchida, Lehmpfuhl & Jäger, 1984; Hsu & Peng, 1987; Wang, Lu & Cowley, 1987). The phenomena of resonance diffraction effects have been observed and studied for many years (Miyake & Hayakawa, 1970; Ichimiya, Kambe & Lehmpfuhl, 1980; Marten & Meyer-Ehmsen, 1985; Lehmpfuhl & Dowell, 1986). In the resonance condition, the specular beam intensity in RHEED can have a sudden increase by a factor of perhaps more than five. The corresponding enhanced reflected beam is often used for imaging in order to increase the intensity and contrast of surface structures (Uchida, Lehmpfuhl & Jäger, 1984) and for recording EELS spectra in order to increase the signal in the spectrum (Wang, Lu & Cowley, 1987). It is therefore important to have a full understanding of surface resonance phenomena.

The condition for the resonance effect is defined by the parabolas in the Kikuchi pattern and is satisfied when the specular beam lies on a parabola. The resonance parabolas have already been described by Ichimiya, Kambe & Lehmpfuhl (1980) based on a simple geometrical consideration. Under the resonance conditions, a diffracted beam parallel, or nearly parallel, to the crystal surface is strongly excited, giving rise to a resonance wave field near the surface region. Based on model calculations using the dynamical RHEED theory, Marten & Meyer-Ehmsen (1985) interpreted the enhancement of the specular beam at the resonance diffraction condition in terms of a monolayer resonance at which electrons are diffracted into bound states of a single atom layer and channel inside the layer before they are diffracted back into the specular beam. On the other hand, based on the similarity between convergent-beam (CB) reflection diffraction patterns and CB transmission diffraction patterns, Lehmpfuhl & Dowell (1986) claimed that resonance is not bound to the surface; it is a three-dimensional effect of the bulk crystal similar to that in transmission diffraction. The enhancement takes place where other Bragg reflections are simultaneously excited. More recently, from analysis of energy-loss spectra, Bleloch, Howie, Milne & Walls (1989) obtained the effective penetration depth both off and on the resonance condition for a GaAs (110) surface. They found that the attenuation depth of the incident wave-field intensity in GaAs for the 880 reflection at 100 keV was typically about 3·3 nm and only reduced very slightly to perhaps 2·5 nm on going into resonance.

In order to obtain a detailed understanding of resonance electron diffraction in RHEED, especially to clarify the controversy concerning the enhancement of the specular beam and the electron penetration into the bulk crystal at both on- and off-resonance conditions, we have performed multislice calculations which can directly simulate the electron wave field in the crystal. The experimental RHEED patterns were also recorded at these conditions for comparison. The main advantage of the multislice method is that the slice used in the simulation is cut in the direction perpendicular to the crystal surface and electron beam propagation such that the electron wave-field distributions near the surface can be output after the electrons have propagated for different distances. The propagation behavior of the electron beam can be traced out. This method has been previously used to simulate dynamical electron scattering in RHEED (Peng & Cowley, 1986; Wang, Lu & Cowley, 1987). However, in these simulations, the dependence of resonance effects on the azimuth angle was not considered and the effects of absorption due to inelastic scattering on elastic scattering were generally included by considering a complex scattering potential field with the imaginary part equal to about 10% of the real part. In our calculations, the effects of inelastic scattering on elastic scattering are neglected for the following reasons: since the electron resonance effect is an effect of elastic scattering, the calculations without inelastic scattering can give us insight into the electron resonance conditions and electron resonance behavior for elastically scattered electrons and the conditions established by such calculations might not be affected by the presence of inelastic scattering; the proper inclusion of the inelastic scattering effect must include the complex potential field and also the presence of the energy-loss electrons which are observed unless excluded by an energy filter, the effects as normally included in the previous calculations (Peng & Cowley, 1986; Wang, Lu & Cowley, 1987) as an effect of absorption makes the electron wave field restricted to the surface and less sensitive to the diffraction conditions, and experimentally there is a lack of data about the exact absorption coefficient which should be appropriately included for a real crystal under the diffraction geometry. Hence, rather than attempting to do this completely it is better to assume elastic scattering only. In our calculations, the dependence of resonance effects on the azimuth angle are also considered.

The simulations and experimental observations are done for 100 keV electrons incident on a perfect GaAs (110) surface in the [001] azimuth for conditions when the 440 and 880 specular reflected beams are on and off resonance conditions, respectively. To a first-order approximation, the resonance conditions are satisfied when the position of the projected centers of the Ewald sphere lies on the parabolas which obey the equation

$$\Theta^2 + \Phi^2 = (\Phi + B_m)^2, \qquad (1)$$

where Θ, Φ are the coordinates of a parabola and B_m is a vector within the reciprocal plane perpendicular to the rods and pointing from the origin to

the mth rod, with m indicating the order of the parabolas. Fig. 1 shows a schematic diagram of parabolas for the GaAs (110) surface in [001] projection, obtained on the basis of a simple geometrical consideration described by Ichimiya, Kambe & Lehmpfuhl (1980). In the figure, the influence of the mean inner potential of the crystal, which is about 14·8 V for GaAs, is not included. These parabolas describing the positions of the projected centers of the Ewald sphere for the resonance conditions can, however, be directly transferred to the diffraction pattern as the parabolas for the specularly reflected spot because of the mirror-related symmetry between the specularly reflected spot and the origin of reciprocal space about the projected centers of the Ewald sphere (Ichimiya, Kambe & Lehmpfuhl, 1980). In reality, the parabola may have a finite width, or may even be split into several components (Marten & Meyer-Ehmsen, 1985; Bird, 1987). The incident condition for resonance, therefore, has an effective resonance region in which the specular beam intensity is enhanced and does not change considerably (Ichimiya, Kambe & Lehmpfuhl, 1980). Two intersection circles of the Ewald sphere with centers at A and B on the first-order parabolas are also shown in the figure which ideally give the resonance conditions for 440 and 880 specular reflections, respectively. In this study, the exact resonance condition which gives the most enhancement of the specularly reflected beam intensity and the effective resonance region are however determined from multislice simulations at different incident angles of the electron beam. The differences of electron distribution near the surface region when electron beams are on resonance and off resonance conditions and the scattering processes involved in RHEED are examined. The corresponding experimental RHEED diffraction patterns for exact resonance and near the resonance conditions have been recorded for comparison.

2. Simulation method

Details of multislice RHEED simulations have been reported previously (Peng & Cowley, 1986; Wang, Lu & Cowley, 1987). The crystal surface is modeled by choosing a unit cell half-filled with atoms. Fig. 2 shows the geometry used in the calculations. The surface modeled is located at plane $y = 0$ in the figure. The program used for the calculations is a modified version of the program due to Ishizuka (1980). The slices are cut in the direction perpendicular to the crystal surface and the z axis with neighboring slices connected by a propagation function, and the effect of the inclined electron beam incident on the surface is considered by projecting the crystal potential along the beam and by modifying the propagation function and interaction constant (Ishizuka, 1982). The incident electron wave in the direction perpendicular to the surface is modeled by a Gaussian-smoothed step function with a width D which can be easily changed in the calculation. Such an electron beam illuminates a finite distance of the surface in the beam direction, which can be estimated as $S = D/\Theta_i$ where Θ_i is the glancing angle of the incident beam. No absorption effect is included in the calculations.

The electron wave field near the surface in the xy plane at different crystal thicknesses z could be output as a two-dimensional distribution in the xy plane or could be output as a profile of intensity distribution along the direction y perpendicular to the surface by integrating the intensity along the x axis. In the latter

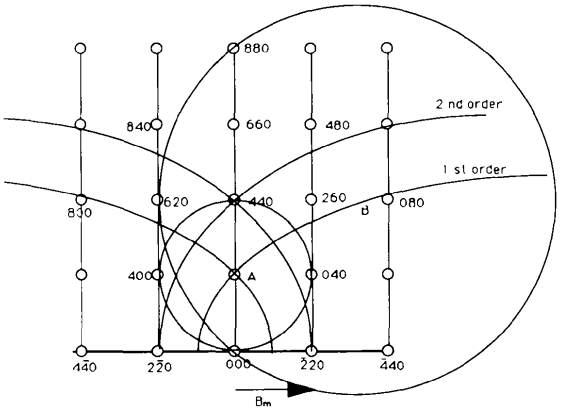

Fig. 1. Schematic diagram showing the parabolas for the GaAs (110) surface in [001] projection. Two intersection circles of the Ewald sphere with centers at A and B on the first-order parabola ideally give the 440 and 880 specular beams in the resonance condition, respectively.

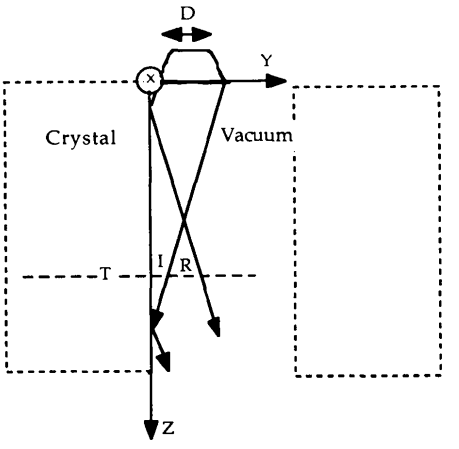

Fig. 2. Schematic diagram showing the geometry used in the simulations.

case, the effective penetration depth of the electron beam into the crystal could be directly determined. The RHEED patterns were calculated by a Fourier transform of the wavefunction. Depending on the crystal thickness z, the electron distribution in the y direction could be roughly divided into three regions indicated by T, I and R, respectively, where T indicates the region inside the crystal where electrons have penetrated through the surface, I is the interference region where the incident electrons and reflected electrons coexist and interfere and R is the region where there are only reflected electrons.

A super unit cell of about 4×160 Å with more than six sampling points per ångström was used to model the surface. A narrow beam of 6 Å was employed in some calculations in order to see how the electron beam propagated after it was incident on the surface at different diffraction conditions. Use of the narrow electron beam, however, causes the transmission beam in the reciprocal space to have a finite size in the direction perpendicular to the surface, which is equivalent to having a beam convergence of about 6 mrad for 100 keV incident electrons. The result of using this narrow beam, therefore, is that a relatively large tilting angle of the incident electron beam is required to get away from a resonance condition to a nonresonance condition. A beam size of 78 Å, which is equivalent to having a convergent angle of 0·4 mrad, was also employed in the calculations, in order to establish the exact resonance condition and the extent of the effective resonance region and to examine the difference in effective penetration depth of electrons and the enhancement of the specularly reflected beam when the incident-beam condition changes from nonresonance to resonance.

3. Experimental

A Philips 400T transmission electron microscope was used in the experimental observations. The (110) GaAs surface used in the study was prepared by cleaving a [001] GaAs wafer. The specimen was then mounted on the goniometer and inserted in the microscope specimen chamber with the cleavage (110) surface nearly parallel to the optical axis of the microscope. The vacuum pressure in the microscope column was ~13 μPa, the specimen was cooled to about 100 K by using liquid nitrogen in order to prevent surface contamination caused by the interaction of the electron beam with hydrocarbon molecules present inside the microscope chamber and to reduce thermal diffuse scattering of the electron beam. A small condenser aperture was used in order to obtain a small convergence angle for the incident beam. The RHEED patterns were recorded from areas without atomic steps to avoid any possible effects due to atomic steps on the RHEED patterns.

4. Results

4.1. 440 *specular beam*

Considering the first parabola in Fig. 1, the 440 specularly reflected beam is ideally on a resonance condition when the projected center of the Ewald sphere lies at point A. This corresponds to a glancing angle of 18·5 mrad for the 100 keV incident electron beam when the refraction effect due to the mean inner potential of the GaAs crystal (14·8 V) is not considered. If we take refraction into account, the angle is about 14·5 mrad. Our first set of calculations using an electron beam with size D of 6 Å was done by changing the glancing angle of the incident beam in steps of 0·5 mrad from 10 to 18 mrad with the azimuth angle fixed at 0 mrad. The profiles of intensity distributions at the different crystal thicknesses, which were obtained by integrating the electron distribution in the xy plane along the x axis, were output as functions of y, with the surface located at $y = 0$ and the positive y pointed toward the vacuum. Figs. 3, 4 and 5 show the electron distributions at crystal thicknesses of 678, 1018, 1357 and 1696 Å for glancing angles of 12·5, 14·5 and 16 mrad, respectively. By comparing the electron distributions at different crystal thicknesses, it is possible to trace out how the electron beam propagates after it is incident on the surface. Propagation of the reflected wave from the surface into vacuum is clearly seen in the figures for crystal thickness of greater than 678 Å. It is found from these calculations that, for an electron beam incident at a small angle (<13 mrad), the electron beam is simply reflected back into vacuum, with very little penetration through the surface atomic layer into the crystal. The reflection angle, which can be easily calculated by measuring the shift of reflected-beam peaks along

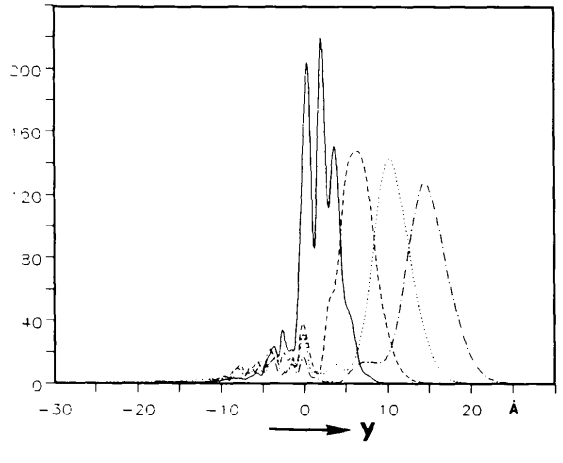

Fig. 3. Profile of electron intensity distributions as a function of y at crystal thicknesses of 678 Å (solid line), 1018 Å (dashed line), 1357 Å (dotted line) and 1696 Å (dashed-dotted line) for an electron beam of size 6 Å incident at glancing angle of 12·5 mrad and azimuth angle of 0 mrad. The surface is located at $y = 0$, with the positive y pointing toward the vacuum.

the y direction as it propagates for different crystal thicknesses, is equal to the incident angle, as might be expected. The intensity in the specular beam is mainly from direct reflection of the incident electron beam from the surface layer of the atoms and is relatively insensitive to the Bragg condition for such a small incident angle. The electron beam starts to penetrate significantly into the crystal only for a relatively large glancing angle (>16 mrad). The glancing angle of 14·5 mrad should give a very favorable situation for the resonance since the surface beams 400 and 040 as well as the specular beam all lie on the Ewald sphere. In fact, a small surface wave field propagating parallel to the surface can be seen in Fig. 4 (as indicated by the arrow). However, only about 20% of the entire electron intensity could penetrate into the crystal to give rise to this resonance effect, the rest of the intensity was directly reflected back into the specular beam. It appears that resonance channeling effects would not produce any significant change in the total reflected intensity. In Fig. 6, we show the profile of the electron distribution at the crystal thickness of 2827 Å using an electron beam with size D of 78 Å incident at the glancing angles of 12·0, 14·5 and 15·5 mrad, respectively. The inset shows the calculated intensity-line scans across the specularly reflected beam under the three conditions. The fringes seen in the vacuum are due to interference between the incident and reflected waves. It is clear that there is practically no penetration of the electron beam beyond the first plane of atoms at the glancing angle of 12·5 mrad and very slight penetration at the glancing angles of 14·5 and 15·5 mrad. The position of the specular beam shifts according to the incident angle as shown in the inset because intensity in the specular beam is mainly due to direct reflection from the surface. The intensity in the specularly reflected beam under the resonance condition is only slightly different from those of nonresonance incident conditions. This would not normally be expected for the resonance effect.

Fig. 7 shows experimental RHEED patterns recorded near the 440 beam in specular reflection with the glancing angle increasing gradually from Figs. 7(a) to (c) and the azimuth angle fixed at 0 mrad. The specular beam in the experimental RHEED patterns

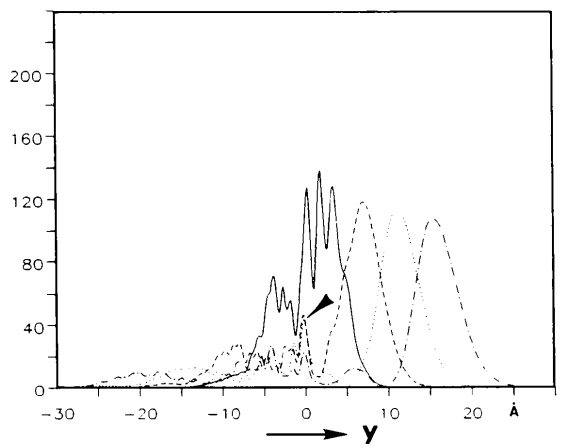

Fig. 4. Profile of electron intensity distributions as a function of y at crystal thicknesses of 678 Å (solid line), 1018 Å (dashed line), 1357 Å (dotted line) and 1696 Å (dashed-dotted line) for an electron beam of size 6 Å incident at glancing angle of 14·5 mrad and azimuth angle of 0 mrad. The surface is located at $y = 0$, with the positive y pointing toward the vacuum.

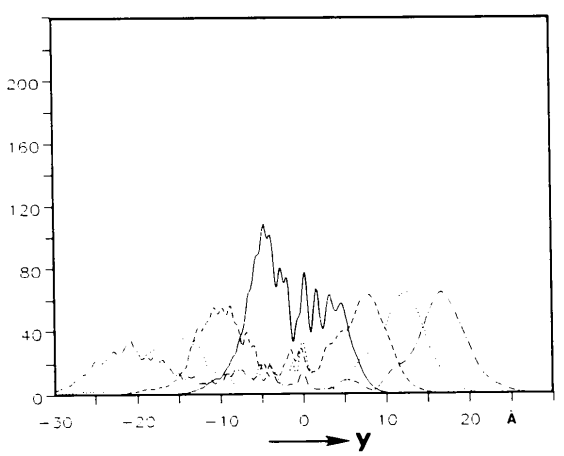

Fig. 5. Profile of electron intensity distributions as a function of y at crystal thicknesses of 678 Å (solid line), 1018 Å (dashed line), 1357 Å (dotted line) and 1696 Å (dashed-dotted line) for an electron beam of size 6 Å incident at glancing angle of 16 mrad and azimuth angle of 0 mrad. The surface is located at $y = 0$, with the positive y pointing toward the vacuum.

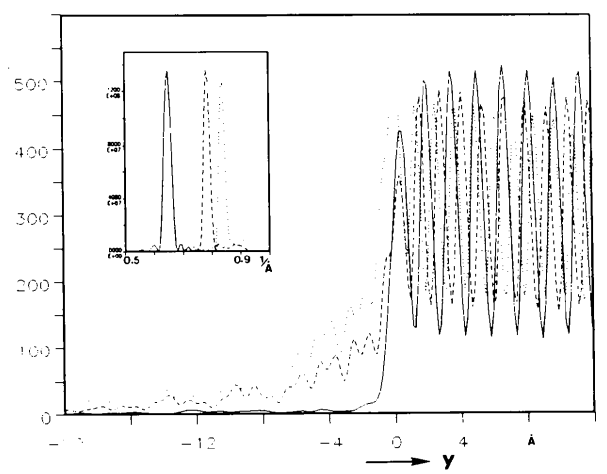

Fig. 6. Profile of electron intensity distributions as a function of y at crystal thickness of 2827 Å for an electron beam of size 78 Å incident at glancing angles of 12·0 mrad (solid line), 14·5 mrad (dashed line) and 15·5 mrad (dotted line) with azimuth angle fixed at 0 mrad. The surface atomic layer is located at $y = 0$, with the positive y pointing toward the vacuum. The inset shows the calculated intensity line scans across the specular beam corresponding to the three incident conditions.

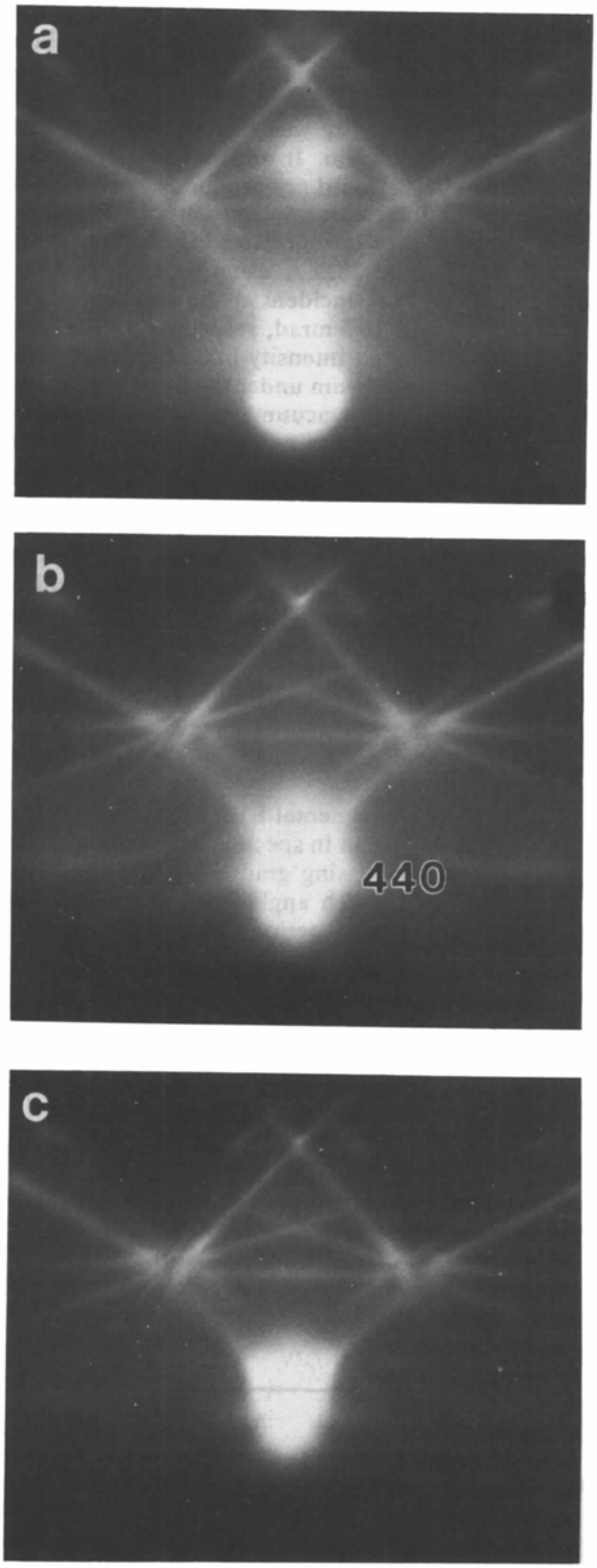

Fig. 7. Experimental RHEED patterns recorded near the 440 beam in specular reflection with glancing angle increasing from (*a*) to (*c*) and azimuth angle fixed at 0 mrad.

is much more diffuse than that calculated for the same incident condition. This difference is probably due to the effect of inelastic scattering. The elongation of the 440 specular beam in the direction perpendicular to the surface in Fig. 7(*b*) might be due to the presence of the small surface wave at the resonance condition. Although it is impossible to make any quantitative comparison between the experimental and theoretical results because of the lack of consideration of inelastic scattering in the calculations, it is clear that the intensity in the specular reflected beam is insensitive to the incident conditions at these small incident angles, which is generally in agreement with the results of the theoretical simulations.

4.2. 880 *specular beam*

Calculations were done by changing the incident-beam angle (both glancing and azimuth angles) with a step of 0·5 mrad near the 880 specularly reflected spot, *i.e.* the projected center of the Ewald circle is near position *B* in Fig. 1. In order to find out the exact incident condition which gives the strongest resonance effect, sensitivity of the resonance effect to the incident-beam condition and effective penetration depth of the electron beam for on and off resonance conditions, a beam with size D of 78 Å was used in the simulations. The strongest enhancement of the 880 specularly reflected beam was found to be at the glancing angle of 35·7 mrad and azimuth angle of 29·7 mrad. Under this condition, the surface 620 beam was strongly excited, a strong wave field was confined in a narrow region near the surface and the 880 specular beam was most enhanced. The glancing angle of 35·7 mrad, after considering the refraction effect due to mean inner potential of the crystal, is the angle that makes the 880 spot near to the Bragg condition.

Fig. 8 shows the profile of the intensity distributions at the crystal thickness of 1583 Å for the glancing and azimuth angles of: (*a*) Θ_r, $\Phi_r - 1{\cdot}5$ mrad; (*b*) Θ_r, Φ_r; (*c*) Θ_r, $\Phi_r + 1{\cdot}5$ mrad; (*d*) $\Theta_r - 0{\cdot}5$ mrad, Φ_r; and (*e*) $\Theta_r + 0{\cdot}5$ mrad, Φ_r; where $\Theta_r = 35{\cdot}7$ and $\Phi_r = 29{\cdot}7$ mrad are the glancing and azimuth angles respectively which give rise to the strongest resonance effect. The surfaces in the figures are located at $y = 0$. The same scales are used in the figures for the convenience of comparison. For the conditions used in Figs. 8(*a*), (*b*) and (*c*), the 880 specular beam is always on the Ewald sphere such that the Bragg condition for the specular beam is satisfied, but great differences in the intensity distributions are seen between the resonance condition and a tilt of the azimuth angle only 1·5 mrad away from resonance. The effective penetration depth is only ~5 Å at the resonance conditions with a very strong surface wave field confined in the first two or three top surface layers and is substantially increased to ~35 Å for the nonresonance conditions. The conditions used in Figs. 8(*d*) and (*e*) make the 880

specular beam not only off the resonance condition but also off Bragg conditions. The general features in Figs. 8(*d*) and (*e*) are, however, similar to those in Figs. 8(*a*) and (*c*) in which the Bragg condition for the specular beam is still satisfied. Fig. 9 shows the calculated RHEED patterns corresponding to the above five incident conditions. The intensity line scans of the 880 specular reflected beam for the five incident conditions are shown in Fig. 10. The 620 surface beam under the resonance condition is strongly excited as can be seen from the RHEED pattern in Fig. 9(*b*), whereas it is very weak off the resonance condition (Figs. 9*a*, *c*, *d* and *e*). The intensity in the specular beam is enhanced by a factor of about five at the resonance condition (curve labeled *b*), as shown by comparing the line scans in Fig. 10. The weak intensity in the specular beam when it is off the resonance condition mainly results from direct reflection from the surface such that the peak of the specular beam shifts in the surface-normal direction according to the change of glancing angle. The effective resonance region for the 880 specular beam can be estimated, based on these simulations, to be ~2 mrad about the azimuth angle and ~1 mrad about the glancing angle. The effective penetration depth of the electrons is very sensitive to small variations of the incident condition. In Fig. 8, it changes from ~5 Å at the resonance condition to ~35 Å for the nonresonance condition.

Fig. 11 shows the RHEED patterns recorded for conditions such that the 880 specular beam is at exact resonance (Fig. 11*b*) and slightly away from resonance by tilting by a small angle of less than 1·0 mrad about the azimuth (Figs. 11*a* and *c*) and glancing

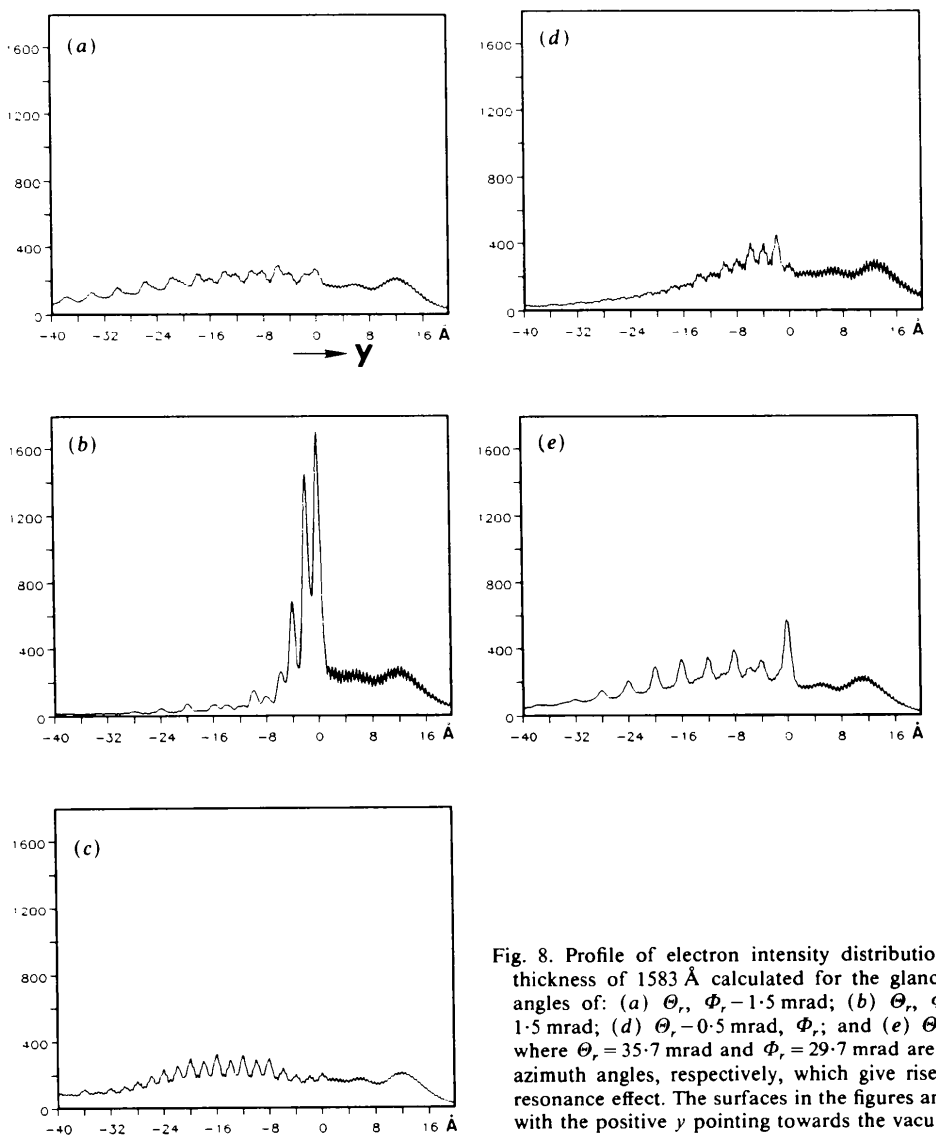

Fig. 8. Profile of electron intensity distributions at the crystal thickness of 1583 Å calculated for the glancing and azimuth angles of: (*a*) Θ_r, $\Phi_r - 1{\cdot}5$ mrad; (*b*) Θ_r, Φ_r; (*c*) Θ_r, $\Phi_r +$ 1·5 mrad; (*d*) $\Theta_r - 0{\cdot}5$ mrad, Φ_r; and (*e*) $\Theta_r + 0{\cdot}5$ mrad, Φ_r; where $\Theta_r = 35{\cdot}7$ mrad and $\Phi_r = 29{\cdot}7$ mrad are the glancing and azimuth angles, respectively, which give rise to the strongest resonance effect. The surfaces in the figures are located at $y = 0$ with the positive y pointing towards the vacuum.

(Figs. 11*d* and *e*) angles. The arrows in the figures indicate the direction of the tilting with respect to the resonance condition. It is clear that the specular beam is enhanced several times at the resonance condition. When the incident beam does not satisfy the resonance condition, the intensity in the specular beam is reduced considerably, even if the Bragg condition for the specular beam is still satisfied as shown in Figs. 11(*a*) and (*c*). The intensity of the 880 specular beam is found to be more sensitive to a small change of the glancing angle than that of the azimuth angle. The effective resonance region for the 880 beam can also be estimated from the observations and is found to be in agreement with the calculations. All these experimental observations seem to be in agreement with the theoretical simulations.

5. Discussion and conclusions

Since inelastic scattering is always present in a real crystal, neglecting the inelastic scattering in our calculations makes a direct comparison between the experimental and theoretical results difficult. However, the electron resonance conditions and effective resonance region obtained from such calculations might not be affected because these are established by the elastically scattered electrons. The presence of inelastic scattering may, however, affect the electron intensity profile inside the crystal obtained under the elastic scattering conditions. Under a resonance condition, the effect of inelastic scattering may cause the electrons which are confined to the first few top surface layers and channel along the surface to dechannel, and thus could effectively increase the penetration depth. Under a nonresonance condition, on the other hand, the electrons penetrating deeply inside the crystal surface may be absorbed due to inelastic scattering, and the effective penetration depth would then be reduced. Including the effect of inelastic scattering on elastic scattering by considering a complex potential field in the calculations could make the electron wave-field distribution inside the crystal insensitive to the diffraction condition, especially if a large imaginary part of the potential (>15%) was used, as shown in the previous calculations (Wang, Lu & Cowley, 1987). In order to properly include inelastic effects in the calculations, both the complex potential field and the presence of the energy-loss electrons must be included. The loss of electron energy is not important, but the angular distribution of the energy-loss electrons needs to be considered. In the calculations with small beam size (6 Å) which implies an

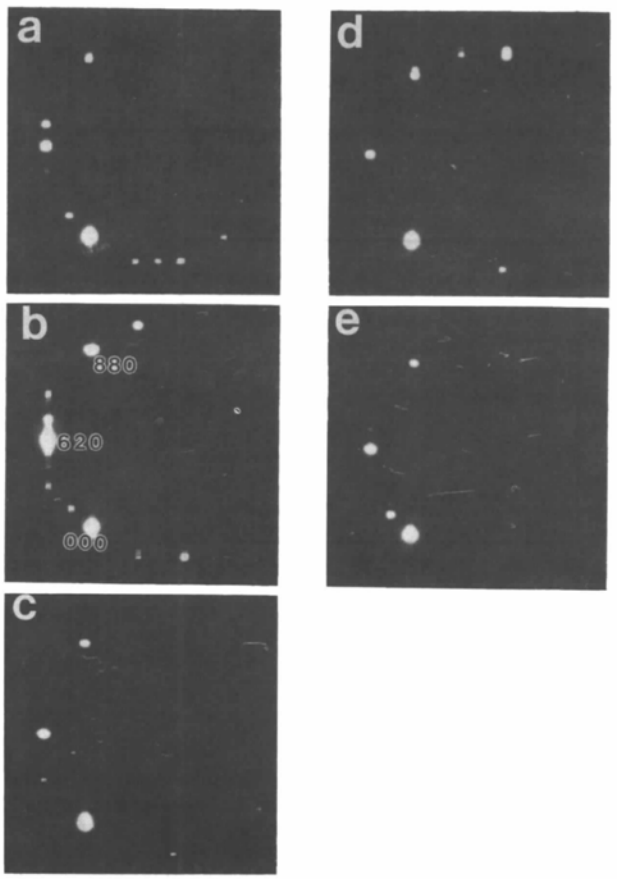

Fig. 9. Simulated RHEED patterns (*a*), (*b*), (*c*), (*d*) and (*e*) corresponding to the five incident conditions used in Figs. 8(*a*), (*b*), (*c*), (*d*) and (*e*), respectively.

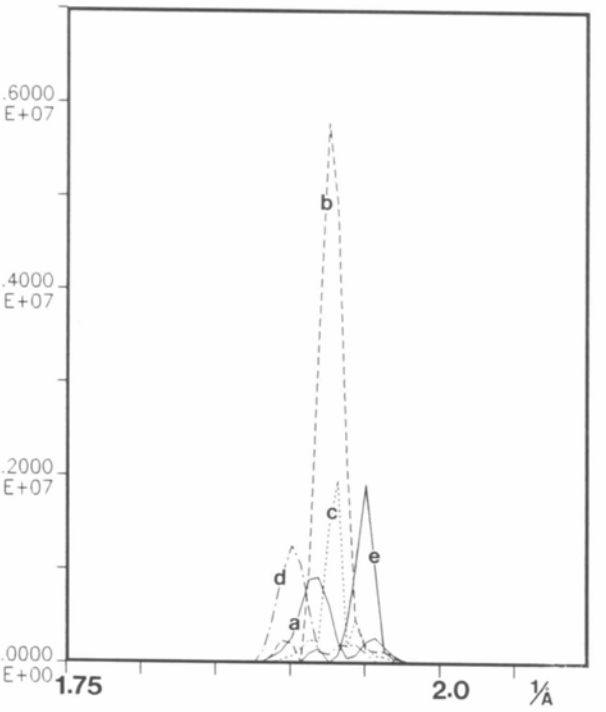

Fig. 10. Calculated intensity line scans (*a*), (*b*), (*c*), (*d*) and (*e*) across the specular beam for the five incident conditions used in Figs. 8(*a*), (*b*), (*c*), (*d*) and (*e*), respectively.

angular spread of about 6 mrad, the effect due to small-angle inelastic scattering such as the inelastic scattering due to plasmons, which has an angular distribution of 1 to 0·1 mrad, can be neglected unless an energy filter is used. However, the complex potential and high-angle scattering due to thermal motion still needs to be included if any quantitative comparisons between the experiment and theory are attempted.

It should also be pointed out that for an electron beam incident at a small angle as simulated for the GaAs 440 spot, a strong coupling between four symmetric beams could cause a broad angular resonance, and the strong reflection from the surface at small incident angles could be due to the resonance effect. However, the calculations using a small-size electron beam (6 Å) indicate this might not be the case for the situations we simulated. At the small incident angles, even in a most favorable resonance condition (Fig. 4), only a very weak surface beam was found to be excited, which was unlikely to give rise to a resonance reflection much stronger than itself. Also,

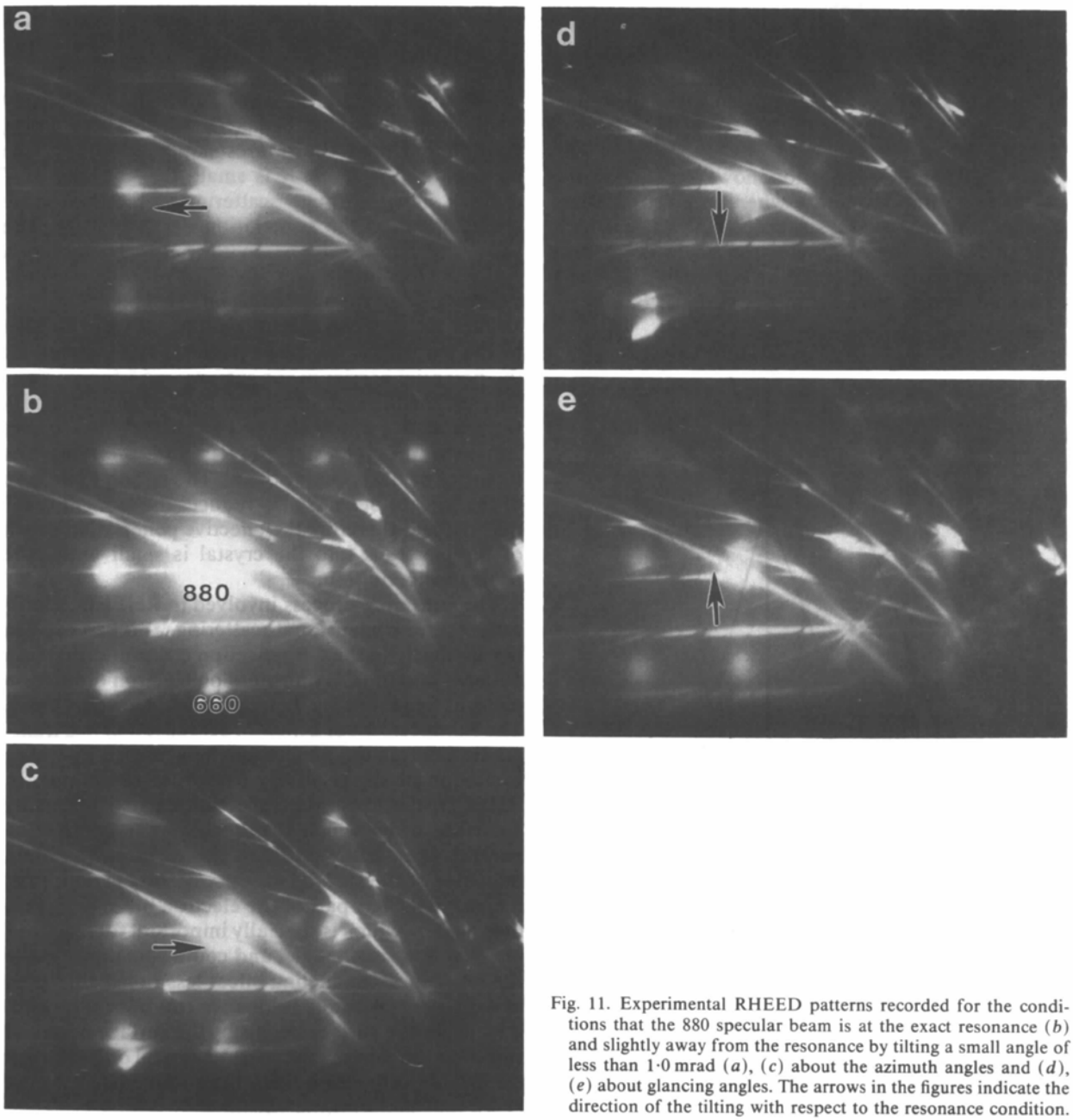

Fig. 11. Experimental RHEED patterns recorded for the conditions that the 880 specular beam is at the exact resonance (*b*) and slightly away from the resonance by tilting a small angle of less than 1·0 mrad (*a*), (*c*) about the azimuth angles and (*d*), (*e*) about glancing angles. The arrows in the figures indicate the direction of the tilting with respect to the resonance condition.

if the resonance was the source of the strong reflection at the small incident angle, in which the electron channeling along the crystal surface was involved, it would be expected that the surface area where the electrons are reflected would be different from where they are incident. With a small-size incident electron beam, the electron propagation after incidence on the surface can be traced out by comparing the electron intensity distributions at the different crystal thicknesses. The results of these calculations, however, show the electrons are mainly reflected from the same area as where they are incident, indicating a strong direct reflection from the surface at the small incident angles. It seems to be necessary to distinguish between a resonance condition and a surface-channeling condition. The resonance condition does not necessarily imply a strong channeling beam along surface layers of atoms to give rise to an enhancement of the reflected beam, this is apparently the case for the small incident angles.

Results from the last section, however, support the following scattering picture when an electron beam is incident onto a crystal surface, as shown schematically in Fig. 12. When an electron beam is incident on a crystal surface, it could be considered as being separated into two beams at the surface: one beam indicated R_1 is generated by direct reflection from the surface; another beam indicated T is the transmission beam which can penetrate through the surface and then be diffracted into all the Bragg directions according to the normal electron scattering in the crystal. The transmission beam could be scattered into the surface beams indicated as S which are propagating parallel or nearly parallel to the surface or scattered into the beam indicated as R_2 which propagates in the same direction as the specular beam and gives its contribution to the specular beam or scattered to any other Bragg direction. The total intensity in the specularly reflected beam indicated as R is therefore the summation of R_1 and R_2. These scattering processes take place simultaneously when an electron beam is incident on a crystal surface. The direct scattering from T to R_2 usually has a higher order than the scattering from T to S and is relatively weak even when the beam R_2 satisfies the Bragg condition. Under the nonresonance condition, the contribution of R_2 to R is small, the intensity of T reduces slowly through scattering to the high-order spots, therefore the penetration depth is large. The scattering from T to S, on the other hand, has a relatively low order, and when the resonance condition is satisfied the surface beam is excited. Since the surface beam, propagating parallel or near parallel to the surface, is localized in the surface region by the potential barrier at the surface and cannot otherwise escape the surface region, the double diffraction from S to R_2, which also has a relatively low order, enhances the intensity of R_2, and therefore the intensity of the specular beam. The strong excitation of the surface beam S also reduces the intensity of T quickly, and therefore the effective penetration depth of the electrons into the crystal is small under the resonance condition.

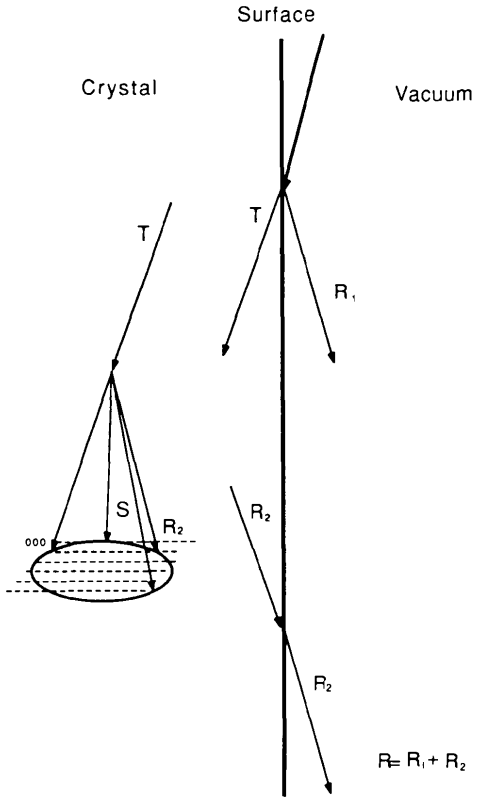

Fig. 12. Schematic diagram showing the scattering processes involved when an electron beam is incident on a crystal surface in the RHEED geometry.

The scattering process involved in RHEED is basically a three-dimensional scattering. This can explain the similarity in the CB reflection electron diffraction patterns and the CB transmission electron diffraction patterns observed by Lehmpfuhl & Dowell (1986). The enhancement of a high-order reflection in a transmission diffraction pattern can be achieved by strong excitation of the relatively low-order reflections. In RHEED, the low-order reflection excited is usually a surface beam which is propagating in a direction parallel or nearly parallel to the surface. The main influence of the surface in the scattering is that: first, it directly reflects part of the electron beam back into the vacuum, which is specially important for electrons incident at a small angle, and could sometimes make the resonance channeling effect less noticeable even in some very favorable resonance conditions; second, it localizes the surface beams by the surface potential such that the electron escapes the crystal only through the double diffraction from the surface beam to the beam reflected into the vacuum.

For the electron beam incident on a surface at a small incident angle, as simulated for the GaAs 440 specular spot, most of the electron intensity of the incident electron beam goes directly into beam R_1, and only about 20% of the intensity goes into the beam T to be diffracted by the crystal. The contribution of R_2 to the total intensity in the specular beam is small even if the resonance condition is satisfied. The total intensity in the 440 specular beam, therefore, is insensitive to the resonance condition. It is found from our simulations and experimental observations that it does not change very much when the incident condition is varied from resonance to nonresonance conditions.

For an electron beam incident on the surface at a relative large angle, such as the cases simulated for the GaAs 880 specular beam near the resonance condition, most of the electron intensity goes into beam T at the surface. The direct reflection (R_1) from the surface is very weak. The direct scattering from T to the 880 reflection (R_2) is weak even when the incident beam satisfies the Bragg condition. The specular beam is, therefore, weak at nonresonance conditions. When the resonance condition is satisfied, the 620 surface beam is strongly excited and localized inside the crystal near the surface by the surface potential and may travel a long distance along the surface. Double scattering from the 620 to the 880 beam (R_2) then enhances the total intensity in the specularly reflected beam. It is found from the simulations and observations that the 880 specular beam is increased by a factor of about five when the incident electron beam satisfies the resonance condition. The effective penetration depth is reduced by exciting the surface beam. According to our calculations, it changes from ~5 Å for the 880 beam at the exact resonance condition to ~35 Å at nonresonance conditions. The enhancement of the 880 specularly reflected beam is very sensitive to the incident condition. The effective resonance region for the 880 specular beam is ~2 mrad about glancing angle and ~1 mrad about the azimuth angle.

Based on analysis of REELS spectra, Bleloch, Howie, Milne & Walls (1989) found that the effective penetration depth for the GaAs 880 reflection at 100 keV only changed slightly from 33 Å at the nonresonance condition to 25 Å at the resonance condition. In their experiments, however, they used an electron beam with illumination angle of about 2 mrad and a collection aperture of about 1·2 mrad, which are comparable to the width of the effective resonance region for the 880 spot. It was therefore very difficult to distinguish the contribution due to resonance from the contribution due to the nonresonance effect. The effective penetration depth obtained from their analysis was actually a weighted average between the effective penetration depth for the nonresonance case and that for resonance. In general, it is necessary to have an electron beam with less convergence and a smaller collecting aperture in order to see the effective penetration depth for the resonance condition. Furthermore, the sensitivity of valence excitation in reflection geometry to the incident-beam condition needs to be tested.

This work has been supported by NSF grants DMR-8514583 and DMR-8810238 and made use of the resources of the Facilities for High Resolution Electron Microscopy at Arizona State University, supported by NSF Grant DMR-8611609. One of the authors (PL) is grateful to Dr D. J. Smith for many useful comments.

References

BIRD, D. M. (1987). *Proc. EMAG Conf.* p. 119. London: Institute of Physics.

BLELOCH, A. L., HOWIE, A., MILNE, R. H. & WALLS, M. G. (1989). *Ultramicroscopy*, **29**, 175-182.

HOWIE, A. (1983). *Ultramicroscopy*, **11**, 141-148.

HSU, T. & PENG, L. M. (1987). *Ultramicroscopy*, **22**, 217-224.

ICHIMIYA, A., KAMBE, K. & LEHMPFUHL, G. (1980). *J. Phys. Soc. Jpn*, **49**, 684-688.

ISHIZUKA, K. (1980). *Ultramicroscopy*, **5**, 55-65.

ISHIZUKA, K. (1982). *Acta Cryst.* A**38**, 773-779.

KRIVANEK, O. L., TANISHIRO, Y., TAKAYANAGI, K. & YAGI, K. (1983). *Ultramicroscopy*, **11**, 215-222.

LEHMPFUHL, G. & DOWELL, W. C. T. (1986). *Acta Cryst.* A**42**, 569-577.

MARTEN, H. & MEYER-EHMSEN, G. (1985). *Surf. Sci.* **151**, 570-584.

MIYAKE, S. & HAYAKAWA, K. (1970). *Acta Cryst.* A**26**, 60-70.

PENG, L. M. & COWLEY, J. M. (1986). *Acta Cryst.* A**42**, 545-552.

UCHIDA, Y., LEHMPFUHL, G. & JÄGER, J. (1984). *Ultramicroscopy*, **15**, 119-129.

WANG, Z. L. & COWLEY, J. M. (1988). *J. Microsc. Spectrosc. Electron.* **13**, 189-204.

WANG, Z. L., LU, P. & COWLEY, J. M. (1987). *Ultramicroscopy*, **23**, 205-222.

YAGI, K. (1987). *J. Appl. Cryst.* **20**, 147-160.